

---

# Supra-Molecular Structure and Chemical Reactivity of Cellulose I Studied Using CP/MAS $^{13}\text{C}$ -NMR

---

Viren Chunilall, Tamara Bush and Per Tomas Larsson

Additional information is available at the end of the chapter

<http://dx.doi.org/10.5772/50673>

---

## 1. Introduction

### 1.1. Chemical cellulose I

In chemical pulping the components that keep wood cells together, mainly lignin are degraded and dissolved in order to obtain fibres for the dissolving pulp and paper processes. The aqueous solutions of pulping chemicals are transferred from the lumen through the cell walls towards the middle lamella and the lignin rich middle lamella, which actually binds the wood cell wall together is dissolved last [1-3]. Cellulose I is the major component of dissolving pulp and constitutes the cell wall of plants and woods. It is the  $\beta$ -1,4-homopolymer of anhydroglucose [4, 5]. Maximising the commercial use of cellulose I dissolving pulp is dependent on developing a clear understanding of its chemical properties as a function of the structural characteristics [6]. The  $\alpha$ -cellulose classification is based on the amount of total hemicellulose and degraded cellulose removed during bleaching. A 96%  $\alpha$ -cellulose sample will typically have low amounts of hemicellulose and degraded cellulose.

#### 1.1.1. Methods of isolation – Acid bisulphite pulping

“In a pulping process, wood is converted into fibres. This can be achieved mechanically, thermally, chemically or through a combination of these techniques” [7]. Chemical delignification, an important process during pulping, results in partial or total removal of lignin from wood by the action of suitable chemicals [8]. The lignin macromolecule is depolymerised through the cleavage of the ether linkages to become dissolved in the pulping liquor. The  $\alpha$ -hydroxyl and  $\alpha$ -ether groups are readily cleaved under simultaneous formation of benzilium ions [9]. The cleavage of the open  $\alpha$ -aryl ether linkages represents

the fragmentation of lignin during acid sulphite pulping. The benzilium ions are sulphonated by attack of hydrated sulphur dioxide or bi-sulphite ions, resulting in the increased hydrophylic nature of the lignin molecule. The extent of delignification depends on the degree of sulphonation as well as the depolymerisation [9].

Sulphurous acid and bi-sulphite ions are the main ingredients during acid bi-sulphite pulping. The sulphite pulping cycle is divided into three phases; the penetration phase, the pulping phase and the recovery phase. Time must be allowed for the chemicals to penetrate the chips completely. The slowest chemical reaction determines the reaction rate [10]. The temperature in the reaction vessel is raised slowly over a period of about 4 hours to 130°C (Penetration phase). Following the penetration phase, the temperature is raised to the maximum, usually between 135°C and 145°C and pulping commences (Pulping phase). The pressure is allowed to rise until it reaches about 800 kPa and then maintained constant by venting. The pulping phase is varied between 43 minutes to 103 minutes depending on the amount of lignin removal required. When the pulping phase ends, the pressure is reduced below 100 kPa during a period of about 90 minutes in order to recover chemicals (Recovery phase). The pulping finishes during the recovery phase. Thereafter the pulp is washed and screened. The total pulping time for acid bi-sulphite pulping is approximately 8.5 hours [10]. The sulphite pulping process takes longer but has a slightly higher yield than the sulphate/'kraft' pulping process [7]. A key advantage of the the sulphate /'kraft' process over the sulphite process is that chemicals used in the pulping liquor can be economically recovered [7]. The sulphite process is however characterised by its high flexibility compared to the sulphate/'kraft' process. In principle, the entire pH range can be used for sulphite pulping by changing the dosage and composition of the chemicals. Thus, sulphite pulping can be used in the production of many different types and qualities of pulp samples for a broad range of applications. The sulphite process can be categorised according to the pH into four different types of pulping namely Acid bi-sulphite, Bi-sulphite, Neutral sulphite (NSSC) and Alkaline sulphate. Table 1 presents the main pH ranges for different sulphite/sulphate pulping processes.

Process	pH	Base	Active reagent	Pulping temperature °C	Pulp yield%	Applications
<b>Acid bi-sulphite</b>	1-2	Ca <sup>2+</sup> , Mg <sup>2+</sup> , Na <sup>+</sup>	SO <sub>2</sub> H <sub>2</sub> O, H <sup>+</sup> , HSO <sub>3</sub>	125 – 143	40 – 50	Dissolving pulp, tissue, printing paper, special paper
<b>Bi-sulphite</b>	3-5	Mg <sup>2+</sup> , Na <sup>+</sup>	HSO <sub>3</sub> , H <sup>+</sup>	150 – 170	50 – 65	Printing paper, tissue
<b>Neutral sulphite (NSSC)</b>	5-7	Na <sup>+</sup> , NH <sub>4</sub> <sup>+</sup>	HSO <sub>3</sub> , SO <sub>3</sub> <sup>2-</sup>	160 – 180	75 – 90	Corrugated medium, semi-chemical pulp
<b>Alkaline sulphate</b>	9 – 13.5	Na <sup>+</sup>	SO <sub>3</sub> <sup>2-</sup> , OH <sup>-</sup>	160 – 180	45 – 60	'Kraft' – type pulp

**Table 1.** pH ranges for different pulping processes [11]

### 1.1.2. Dissolving pulp

The unbleached pulp that results after acid bi-sulphite pulping is used as raw material for dissolving pulp production. Lignin and hemicelluloses in the unbleached pulp are considered to be contaminants and are removed in order to produce high purity dissolving pulp samples. This can be done using oxygen delignification followed by a 4 step bleaching sequence. The bleaching sequence can either be Chlorine dioxide – Alkali extraction – Chlorine dioxide – Hypochlorite ( $\text{D}_1\text{ED}_2\text{H}$ ) or Chlorine dioxide – Alkali extraction – Chlorine dioxide – Peroxide ( $\text{D}_1\text{ED}_2\text{P}$ ) stage depending on the desired end product i.e. 91% $\alpha$ , 92% $\alpha$  or 96% $\alpha$  dissolving pulp samples. “Dissolving pulp is a chemical pulp intended primarily for the preparation of chemical derivatives of cellulose. It is utilized for the chemical conversion into products such as microcrystalline cellulose, cellophane, cellulose acetate, cellulose nitrate” [7].

### 1.1.3. Characterisation of cellulose I

There are a few traditional methods of analysing the chemical properties of cellulose I. Some of these methods include the Permanganate number determination, which is used to obtain the lignin content of the pulp [12]. The acid insoluble lignin content (Klason lignin) in wood and raw pulp is determined by gravimetric analysis [13]. The viscosity of a pulp sample provides an estimate of the degree of polymerisation (DP) of the cellulose chain. Viscosity determination of pulp is one of the most informative procedures that is carried out to characterise a polymer i.e. this test gives an indication of the degree of degradation (decrease in molecular weight of the polymer, i.e. cellulose) resulting from the pulping [14]. Pulping is known to affect cellulose structure by the generation of oxidised positions and subsequent chain cleavage in pulp samples [15]. The copper number thus gives an indication of the reducing end groups in a pulp sample [16]. Low molecular weight carbohydrates (hemicellulose and degraded cellulose) can be extracted from pulp samples with sodium hydroxide. The solubility of a pulp in an alkaline solution thus provides information on the degradation of cellulose and loss or retention of hemicellulose during the pulping and bleaching processes.  $S_{10}$  (%) and  $S_{18}$  (%) indicate that proportion of low molecular weight carbohydrates that are soluble in 10% and 18% sodium hydroxide respectively.  $S_{10}$  (%) alkali solubility gives an indication of the total extractable material i.e. degraded cellulose/short chain glucan and hemicellulose content in a pulp sample.  $S_{18}$  (%) alkali solubility gives an indication of the total hemicellulose content of the pulp sample and is also known as the percentage gamma ( $\gamma$  %) cellulose content of pulp samples [17]. The monosaccharide constituents (glucose, mannose, xylose, arabinose etc.) can be analysed using high performance liquid chromatography coupled with pulsed amperometric detection [18]. The concentrations of the monosaccharide constituents are obtained from the calibration curves of the standards (glucose, mannose, xylose, arabinose etc.). Molecular weight distribution analysis can be performed using Size Exclusion Chromatography coupled with Multi-Angle Laser Light Scattering (SEC-MALLS) on fully bleached 91% $\alpha$ , 92% $\alpha$  and 96% $\alpha$  samples after conversion to cellulose nitrate [19]. Due to its capability of

measuring a sample in its native state, CP/MAS  $^{13}\text{C}$ -NMR can be applied to investigate both the chemical and physical structure of lignocellulosics [3]. It is characteristic of NMR spectra that chemically equivalent carbons can be distinguished if they reside in magnetically non-equivalent surroundings. So even though the corresponding carbons of different anhydroglucose units of cellulose are chemically similar, they can be distinguished in a CP/MAS  $^{13}\text{C}$ -NMR spectrum if they are in different magnetic environments, due to different packing of the cellulose chains or distinct conformations. Separate signals for crystalline and non-crystalline carbons as well as splitting of crystalline signals can thus be detected [20].

*1.1.4. The concept of reactivity coupled to the different grades of dissolving pulp i.e. 91%, 92% and 96%  $\alpha$ -cellulose for commercial products viz. microcrystalline cellulose, viscose and cellulose acetate respectively.*

The ‘reactivity’ of cellulose can refer to its capacity to participate in diverse chemical reactions. Each anhydroglucose unit in a cellulose polymer has three different hydroxyl groups. The hydroxyl groups at O(2) H, O(3) H and O(6) H are the main reactive groups susceptible to chemical modification [21]. When discussing reactivity of cellulose I, the accessibility of the hydroxyl groups on the surface of fibrils or fibril aggregates to the chemical reagents is a crucial factor [4]. This accessibility is limited by the compact structure of cellulose I, which is determined by the presence of highly ordered regions formed by strong hydrogen bonds [10].

With the advent of infrared spectroscopy, accessibility could be determined by deuteration [22]. The O(3)H can be described as ‘unreactive’ when the cellulose surface is highly ordered and ‘reactive’ when the cellulose surface is less ordered [21]. Authors of [21] used the procedure described in [23] to calculate the availability of surface hydroxyl groups. More recently investigators reported a Fourier Transform Infrared (FTIR) spectroscopic method to measure the accessibility and size of cellulose fibrils from the cell wall of *Valonia ventricosa* by investigation of deuteration and rehydrogenation [24]. Investigators proposed that the accessibility of cellulose I depends on the amount of surface that is accessible, as determined by the size of cellulose fibril aggregate, the structure of the cellulose molecules, which will determine which hydroxyl groups are accessible; as well as the size and type of reagent [4]. The method used in this study for assessing cellulose I structure and accessibility was to determine the dissolving pulp reactivity during cellulose derivative formation.

Acid hydrolysis performed on cellulose I rich fibres can serve as one illustration of the relationship between cellulose supramolecular structure and reactivity. Cellulose I isolated from several sources was subjected to acid hydrolysis by hydrochloric acid, 2.5 M HCl (aq) at 100 °C for up to 17 h with reflux [6, 25, 26]. In the case of isolated cellulose I consisting of thinner fibril aggregates, such as cellulose isolated from wood and cotton, a 17 h hydrolysis resulted in the complete conversion to a sol of cellulose nano-particles. This was not observed for cellulose I isolated from *Cladophora sp.*, after a 17 h hydrolysis a fibrous material remained (unpublished data). The lower susceptibility towards acid hydrolysis exhibited by the *Cladophora* cellulose correlates well with the comparatively larger lateral

cellulose dimensions. The larger lateral cellulose dimensions result in a low specific surface area which could, at least in part, account for the comparatively low reactivity observed for the *Cladophora* cellulose.

In the case of the 92%  $\alpha$ -cellulose pulp the typical final product is synthetic spun textile fibres manufactured after dissolution of the dissolving pulp fibres. Here, the fibre material's 'reactivity' can be considered to be indicative of how easily the fibres can be dissolved in a solvent system. During the initial stage of the dissolution process, solvent needs to be transported into the pore system of the cellulose I rich fibres, and the subsequent dissolution of cellulose liberates polymers or colloidal particles from the fibre material. In such a system both the lateral dimensions of the cellulose (inversely proportional to the specific surface area) and the pore size characteristics of the fibre wall can influence the 'reactivity' or the ease of dissolution of the cellulose fibre. Depending on the lateral dimensions of the cellulose structure to be dissolved and the typical pore size, the dissolution process may become limited by transport processes. If cellulose structural elements are large and the average pore size of the fibre wall is small, the material liberated by the solvent may close up pores needed for transport of the incoming solvent and for transport of dissolved cellulose out of the fibre wall. This can serve as another illustration of how the cellulose supramolecular structure can affect the cellulose 'reactivity'. In this Chapter, cellulose acetates were produced by heterogenous acetylation from bleached acid bisulphite pulp fibres using a mixture of acetic acid and acetic anhydride in the presence of sulphuric acid catalyst. The degree of acetylation was observed as a function of reaction time and characterised by solid state CP/MAS  $^{13}\text{C}$ -NMR.

## 1.2. CP/MAS $^{13}\text{C}$ -NMR for determining cellulose I structure and 'reactivity'

### 1.2.1. Principles of CP/MAS $^{13}\text{C}$ -NMR spectroscopy

CP/MAS  $^{13}\text{C}$ -NMR spectroscopy is a useful technique for studying the structure of semi-crystalline polymorphic solids. CP/MAS  $^{13}\text{C}$ -NMR has not always been used for structure determination because of line broadening. Broad lines characteristic of conventional NMR measurements on solid samples is attributed to two causes, static dipolar interactions between  $^{13}\text{C}$  and  $^1\text{H}$  and the chemical shift anisotropy. The strong dipolar interaction between  $^{13}\text{C}$  and neighbouring protons can be removed by high-power proton decoupling. The second cause of line broadening, the chemical shift anisotropy is experimentally diminished by Magic Angle Spinning (MAS), which incorporates a rapid spinning (5 - 15 kHz) at an angle of 54.7 degrees with respect to the external magnetic field. Magic angle spinning will also average any residual dipolar broadening [27]. Cross-Polarization (CP) is a pulse technique used to enhance the signal-to-noise ratio of the spectrum, since  $^{13}\text{C}$  is a low abundance nuclei with a comparatively small gyromagnetic ratio and its spin-lattice relaxation in solids is long [28]. This enhancement is performed by first exciting the  $^1\text{H}$  spins and then transferring the magnetism to the  $^{13}\text{C}$ -spin system [28]. Cross-polarization in combination with magic angle spinning and high power proton decoupling generates spectra with comparatively high resolution and good sensitivity [28]. Typical CP/MAS  $^{13}\text{C}$ -

NMR spectra from cellulose I are made up of six signals from the anhydroglucose unit split into fine structure clusters due to the supra-molecular structure of the cellulose I fibril (Figure 1). The information content in this fine structure is high, but the accessibility of the information is hampered by a severe overlap of the signals [6]. In order to obtain quantitative information on the supra-molecular structure of cellulose, post-acquisition processing (spectral fitting) of the spectra is needed [25].

### 1.2.2. CP/MAS $^{13}\text{C}$ NMR in combination with spectral fitting

Figure below, shows significant differences are observable in the CP/MAS  $^{13}\text{C}$ -NMR spectra of the same polymer,  $\beta$  1- $\rightarrow$ 4, D-glucan isolated from different sources. These differences are attributed to differences in the supramolecular structure or polymer chain packing of the samples. Since there is significant signal overlap within each spectrum the desired information is not directly available. For this reason a post-acquisition processing method was developed based on non-linear least squares fitting of spectra. Using this method at least two things are required; an interpretation of a representative part of the spectrum and a mathematical model describing the functions used to model the recorded signals [25, 26, 29]. A spectral interpretation of the C4 spectral region was made possible by combining a model for the structural elements of cellulose possessing square cross-sections with a mathematical model comprising two distinct kinds of functions; Lorentzian and Gaussian [25]. The basic features of the mathematical model are that all non-crystalline states of polymer order are described as Gaussian functions and polymers located in the crystalline forms of cellulose are assigned Lorentzian functions (Figure 2). The rationale for the need for two kinds of mathematical functions for describing spectra recorded on semi-crystalline cellulose has been described in a recent paper [29].

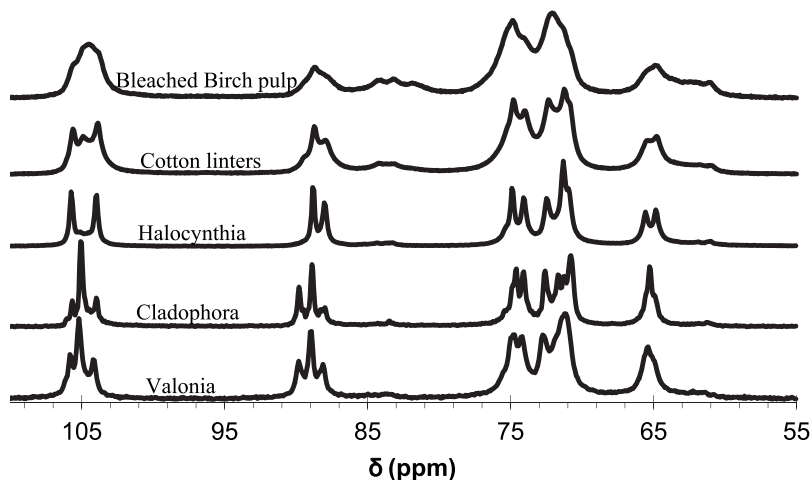


**Figure 1.** CP/MAS  $^{13}\text{C}$ -NMR spectra of cellulose I isolated from different sources. From bottom to top the order is: Valonia cellulose, Cladophora cellulose, Halocynthia cellulose, cotton linters and bleached birch pulp

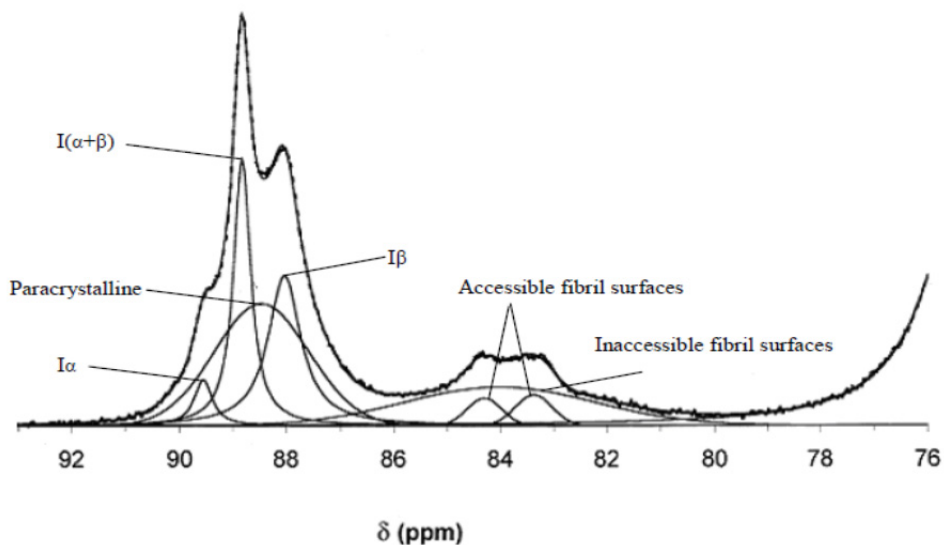


**Figure 2.** The fitting of the C-4 region of a CP/MAS  $^{13}\text{C}$ -NMR spectrum recorded

The interpretation of the CP/MAS  $^{13}\text{C}$ -NMR spectra has been further substantiated by  $^{13}\text{C}$  enriched Cellulose I samples [30].

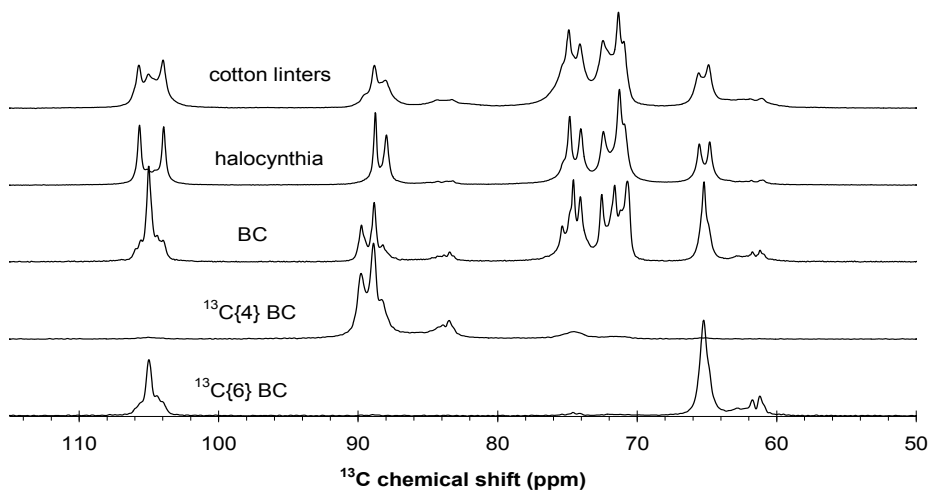


**Figure 3.** Illustrating the effect of  $^{13}\text{C}$  enrichment obtained in bacterial Cellulose I obtained by cultivating bacteria (*Gluconacetobacter xylinus*) in the presence of glucose selectively  $^{13}\text{C}$  enriched in the C4 and the C6 position.

Figure 3 shows spectra recorded on Cellulose I isolated from cotton linters, Halocynthia, bacterial cellulose (BC),  $^{13}\text{C}\{4\}$ BC is spectra recorded on bacterial cellulose cultivated from a medium containing glucose selectively enriched in the C4 position, and  $^{13}\text{C}\{6\}$  BC is spectra recorded on bacterial cellulose cultivated from a medium containing glucose selectively enriched in the C6 position. The occurrence of the enriched signal intensity from the C1 position (about 105 ppm in the bottom spectra is due to scrambling during the biosynthesis [30].

### 1.2.3. Cellulose I fibril aggregate model

A model of aggregated cellulose I fibrils was constructed based on spectral fitting and spin diffusion experiments (Figure 4) [31]. Two C-4 signals at 84.3 and 83.3 ppm are assigned to cellulose at accessible fibril surfaces in contact with water and the C-4 signal at 83.8 ppm is assigned to cellulose at water-inaccessible fibril surfaces, formed either by interior distortions or aggregation of fibrils [32]. Paracrystalline cellulose can, at least in part, be explained by the presence of phase boundaries, such as the fibril-to-fibril contact surfaces. The finite lateral dimensions of the cellulose I fibril results in the presence of surfaces (phase boundaries) where the polymer conformation deviates from the conformation found for polymers located in the crystalline interior of the fibril. This result in well separated NMR signals from the C4 atoms located in the fibril interior and the C4 atoms located on the fibril surfaces, a 4 to 5 ppm shift difference is typically observed between the two. The responsible conformational differences may disappear gradually towards the fibril centre, resulting in the presence of polymers in a conformation intermediate between that of the fibril surfaces and the fibril interior; denoted para-crystalline cellulose. This is schematically illustrated in Figure 3 where the paracrystalline cellulose is shown to penetrate one layer below the fibril-to-fibril contact surface. This is purely an arbitrary representation since penetration depth is dependent on the size and severity of the distortions induced at the fibril surfaces, and paracrystalline cellulose may also be present beneath the accessible fibril surfaces [31].

It may be pointed out that the terminology used for describing the different states of order of the glucan polymers situated in the cellulose I fibril and fibril aggregate is quite distinct from the terminology used when interpreting results obtained from X-ray diffraction recorded on cellulose samples. However the two sets of terminologies can be reconciled if the degree of crystallinity as determined by X-ray diffraction techniques is compared with the degree of crystallinity computed from the NMR signal intensity originating from the crystalline plus the para-crystalline moieties. This way a reconciliation of the X-ray term “amorphous cellulose” and the corresponding NMR term “non-crystalline cellulose” immediately become obvious by relative signal intensity closure for both methods. The signal intensity detected as amorphous cellulose in the case of X-ray diffraction, is detected and described as non-crystalline cellulose in the case of NMR. This means that the sum of NMR signal intensities from accessible and inaccessible fibril surfaces corresponds to the X-ray estimate of amorphous cellulose. Experimental evidence that supports this reconciliation of NMR and X-ray terminology can be found in [33] where a good agreement was found when the degree of crystallinity and lateral fibril dimensions of cellulose in bleached kraft pulp was determined by both X-ray diffraction



and NMR. Such an agreement between results obtained by X-ray and NMR is only possible if the above reconciliation of terminologies and measurements results are correct.

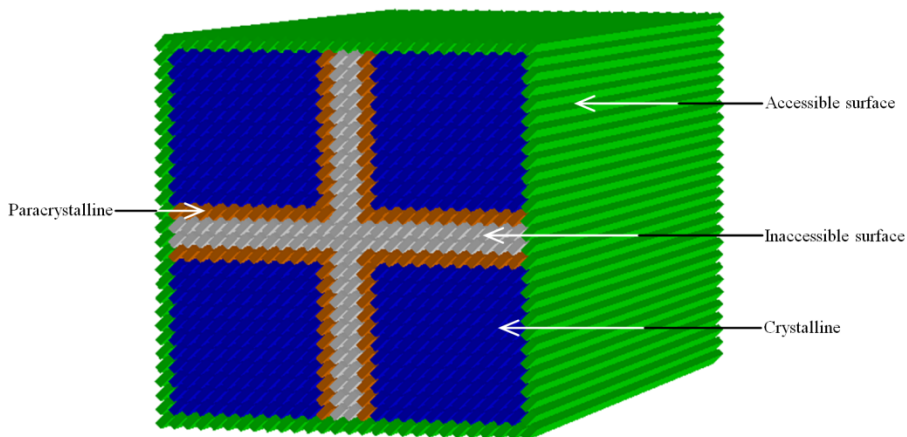


**Figure 4.** Schematic model of four aggregated cellulose I fibrils

#### 1.2.4. The application of CP/MAS <sup>13</sup>C-NMR for determining average lateral fibril dimensions (LFD) and lateral fibril aggregate dimensions (LFAD)

Fibrils have cross-sections of varying shape and width in the range from a few nanometers to a few tenths of nanometers [4, 10, 34]. There is a broad distribution of fibril aggregate structures in pulp probably due to the presence of hemicelluloses and short chain glucan in pulp samples. In order to calculate the average lateral fibril dimensions (LFD) and average lateral fibril aggregate dimensions (LFAD), spectral fitting has to be performed on lignin- and hemicellulose-free pulp samples (glucose content > 95 %) since interfering signals (signal overlap from hemicellulose and spinning side bands from the lignin) influence calculations [32]. From the assignment of the signals in the C-4 region of the CP/MAS <sup>13</sup>C-NMR spectra, lateral dimensions can be assigned. Assuming a square cross-section (Figure 4), the fraction of the signal intensity from accessible fibril surfaces (calculation of lateral fibril aggregate dimension) or the fraction of the signal intensity from accessible and inaccessible fibril surfaces (calculation of lateral fibril dimensions) are both denoted  $q$  and are given by the equation:

$$q = \frac{(4n-4)}{n^2} \quad (1)$$

where  $n$  is the number of cellulose chains on the side of the square fibril or fibril aggregate cross-sections. A conversion factor of 0.57nm width per cellulose polymer has been used in the calculations [35-37]. The final 91%, 92% and 96%  $\alpha$ -cellulose dissolving pulp samples were initially run on the CP/MAS <sup>13</sup>C-NMR in the wet state (never dried). The samples were then subject to drying via two strategies, viz. oven and condition drying. Oven dried pulp samples were prepared by placing dissolving pulp into the oven at 104°C for 18 hours.

Condition dried pulp samples were prepared by placing pulp in a conditioned room at 23°C with 50% RH for 5 days. The dried pulp samples were re-wetted and analysed by CP/MAS  $^{13}\text{C}$ -NMR. Table 2 shows the LFAD measurements of the never dried pulp samples and the pulp samples after condition drying and oven drying.

Pulp sample	$S_{10}$ (%)	$S_{18}$ (%)	$S_{10} - S_{18}$ (%)	LFAD <sub>NMR</sub> (nm)		
				Never dried	Condition dried	Oven dried
91% $\alpha$ -cellulose	11.4	5.9	5.5	17.5 $\pm$ 0.6	21.2 $\pm$ 1.6	26.1 $\pm$ 1.9
92% $\alpha$ -cellulose	9.1	4.6	4.5	18.3 $\pm$ 0.5	22.3 $\pm$ 1.6	28.0 $\pm$ 2.1
96% $\alpha$ -cellulose	6.7	2.4	3.3	22.5 $\pm$ 0.7	28.0 $\pm$ 2.6	34.7 $\pm$ 2.6

**Table 2.** Total extractable material  $S_{10}$  (%), LFAD (nm), of final dissolving pulp samples subject to different drying strategies

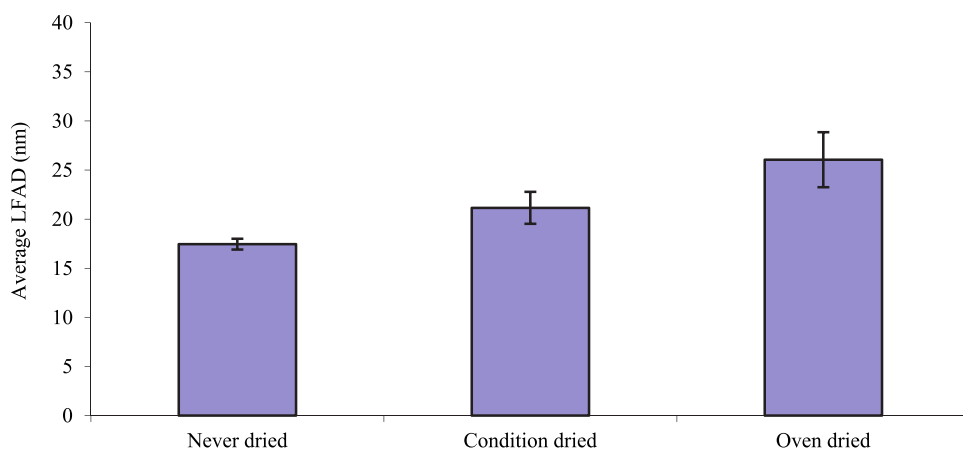


**Figure 5.** Average LFAD (nm) for the '91%  $\alpha$ -cellulose' using the different drying strategies

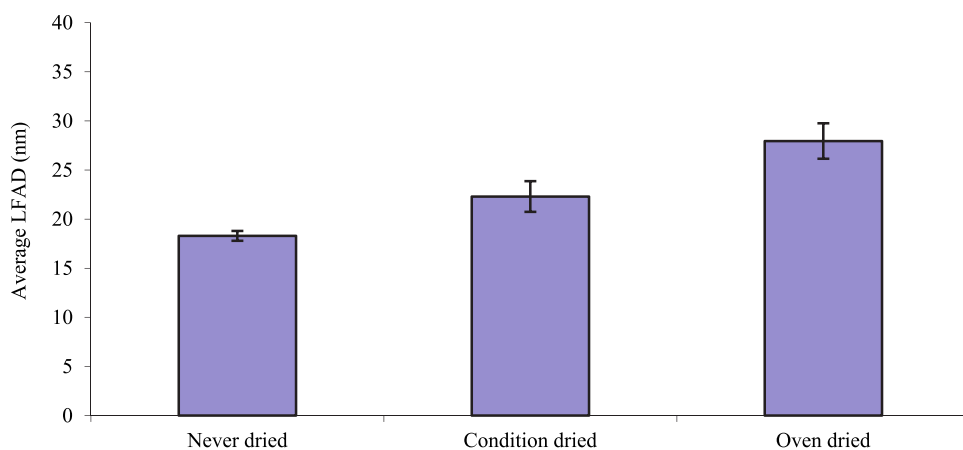


**Figure 6.** Average LFAD (nm) for the '92%  $\alpha$ -cellulose' using the different drying strategies

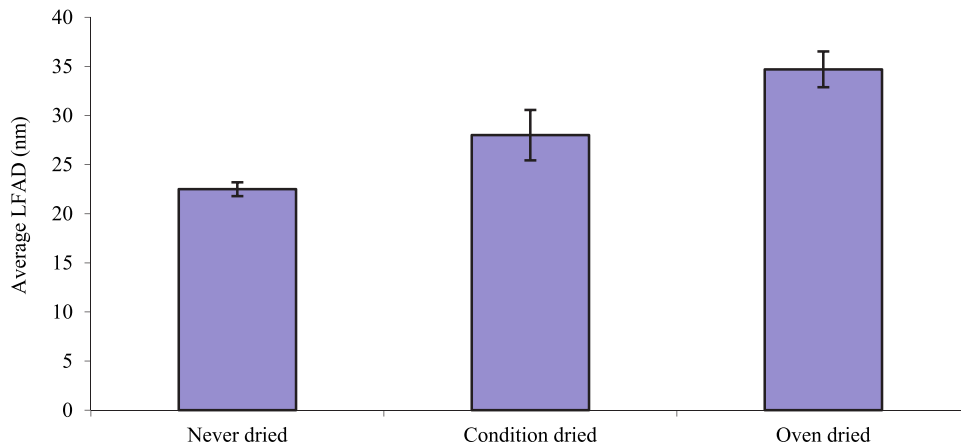


**Figure 7.** Average LFAD (nm) for the '96%  $\alpha$ -cellulose' using the different drying strategies

Inspection of the data in Table 2 shows that there was a change in LFAD upon condition drying e.g.  $17.5 \pm 0.6$  nm to  $21.2 \pm 1.6$  nm for the 91%  $\alpha$ ;  $18.3 \pm 0.5$  nm to  $22.3 \pm 1.6$  nm for the 92%  $\alpha$  and  $22.5 \pm 0.7$  nm to  $28.0 \pm 2.6$  nm for the 96 $\alpha$ . The 91%  $\alpha$  and 92%  $\alpha$ -cellulose pulp samples (Figures 5 and 6) show an increase in lateral fibril aggregation upon oven drying,  $17.5 \pm 0.5$  nm to  $26.1 \pm 1.9$  nm and  $18.3 \pm 0.5$  nm to  $28.0 \pm 2.1$  nm respectively. The 96%  $\alpha$  pulp sample (Figure 7) shows an increase in aggregate dimensions from  $22.5 \pm 0.7$  nm to  $34.7 \pm 2.6$  nm. Although the three grades of pulp samples show similar trends upon oven drying, the increase in aggregate dimensions is the largest during oven drying. The increase in LFAD was greater for the 96% $\alpha$ -cellulose followed by the 92% and 91%  $\alpha$ -cellulose with the aggregate dimensions being  $34.7 \pm 2.6$  nm,  $28.0 \pm 2.1$  nm and  $26.1 \pm 1.9$  nm respectively. First time drying, oven or condition drying, induced a degree of irreversible aggregation of the cellulose fibrils i.e. 'hornification'. Hornification, a term introduced by Jayme [38], is used in wood and pulp literature to describe the 'stiffening of a polymer structure' taking place in lignocellulosic (cellulose containing lignin) material upon drying or water removal [39]. Wetting the samples, prior to running on the CP/MAS  $^{13}\text{C}$ -NMR, does not return the LFAD to the original never dried state hence aggregation is irreversible.

The results thus far point to the possibility of controlling LFAD by using different drying strategies. Condition drying the pulp samples is a possible method that can be used to control fibril aggregation. Oven drying presents a relatively rapid form of drying where the high temperature e.g. during oven drying ( $104^\circ\text{C}$ ) increases the rate at which water is removed and the movement of the fibrils. This possibly leads to a random restructure of the fibril aggregates and an increase in lateral fibril aggregate dimension. If LFAD can be controlled then it can be used to provide dissolving pulp samples with pre-defined specific surface area. Since the extractable hemicellulose and degraded cellulose/short chain glucan content influence the LFAD during acid bi-sulphite pulping and bleaching, there is a possibility that it can have an influence on fibril aggregation during drying. This increase in aggregate dimensions upon drying is supported by LFAD results obtained on other

*Eucalyptus* pulp samples investigated recently [40]. An increase in aggregate dimension due to drying seems to correlate with the total extractable material  $S_{10}$  (%) i.e. hemicellulose [ $S_{18}$  (%)] and degraded cellulose/short chain glucan [ $S_{10} - S_{18}$  (%)]. During drying, an increased contact between the cellulose fibril surfaces is established [41, 42], and it seems that the dissolving pulp samples with a high total extractable material (i.e. 11.4 - 91%  $\alpha$ -cellulose) have a lower tendency for cellulose fibrils to aggregate during drying. A possible explanation for the phenomenon, i.e. an increase in aggregate dimensions upon drying, is shown in Figure 8 and Figure 9 below.

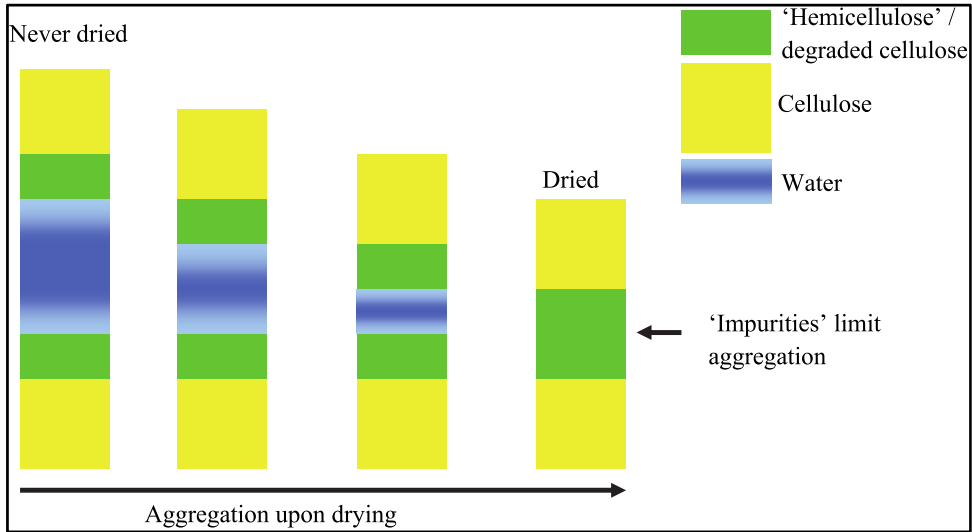


**Figure 8.** Aggregation of fibrils in the presence of extractable hemicellulose and/or degraded cellulose/short chain glucan.

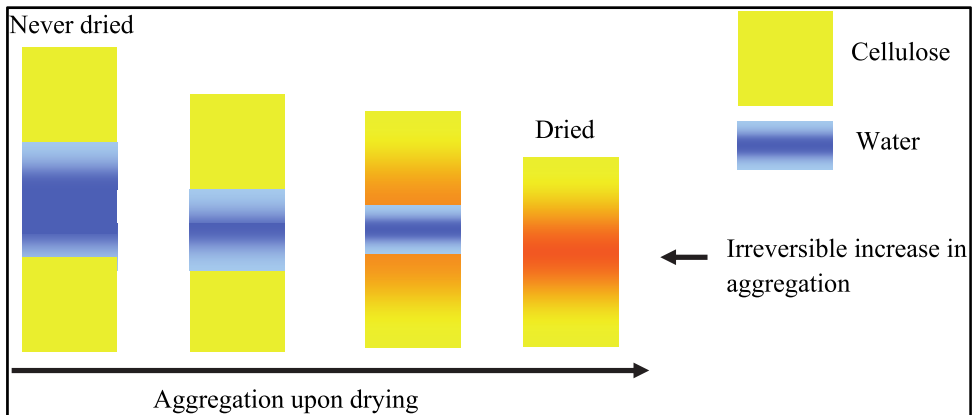


**Figure 9.** Aggregation of fibrils in the absence of extractable hemicellulose and/or degraded cellulose/short chain glucan

Drying pulp samples results in an irreversible change in lateral fibril aggregate dimensions irrespective of the drying strategies employed. The change can be marginal, as in the case of condition drying, or substantial as in the case of oven drying the pulp samples. Figure 8 shows the aggregation of fibrils upon drying in the presence of the total extractable content  $S_{10}$  (%) i.e. hemicellulose and degraded cellulose/short chain glucan ('impurities'). It is however evident, Figure 9, that the measurement of the fibril dimension for the dried material is going to be similar to the never dried material due to the presence of significant amounts of 'impurities'. Investigators recently showed that the presence of 4-O-methylglucuronxytan in the pulp samples diminishes the fibril aggregation and hence hornification during drying [43]. This scenario resembles that prevalent in the 91% $\alpha$  and 92% $\alpha$  pulp samples where the presence of extractable hemicellulose and degraded cellulose/short chain glucan could possibly affect fibril aggregation. The second scenario, Figure 9, shows the aggregation of fibrils upon drying in the absence of 'impurities' or in the presence of small quantities amounts of 'impurities'. Drying removes water from pores between the cellulose molecules facilitating their aggregation, however the absence or presence of small quantities of 'impurities' does not prevent the aggregation of fibrils. This scenario resembles the drying of 96% $\alpha$  pulp where small quantities of extractable hemicellulose and degraded cellulose/short chain glucan do not inhibit the aggregation of fibrils. While this study shows the changes in LFAD upon drying in the radial direction of the fibril, there have been studies that showed that relatively pure forms of cellulose (cellulose nanocrystals) also experience changes in the longitudinal direction upon drying [44].

#### 1.2.5. Computation of specific surface area from LFAD

The average density of cellulose molecule is approximately 1500 kg/m<sup>3</sup> i.e.  $\rho \approx 1500$  kg/m<sup>3</sup>. The length along one side is taken as  $a$  in meters (m) and the longitudinal length of the cellulose molecule is taken as  $L$ . The total surface area ( $A$ ) is thus given as:

$$A = a \times L \times 4 \quad (2)$$

The volume occupied by the cellulose molecule is given as:

$$\text{Volume: } V = a^2 \times L \quad (3)$$

With the mass of the cellulose molecule given as:

$$\begin{aligned} \text{Mass: } M &= V \times \rho \\ &= a^2 \times L \times \rho \end{aligned} \quad (4)$$

Hence the specific surface area (surface area per unit mass) can be calculated as:

Specific surface area

$$\begin{aligned} (\sigma) \frac{A}{M} &= \sigma = \frac{a \times L \times 4}{a^2 \times L \times \rho} \\ &= \frac{4}{\rho \times a} \end{aligned} \quad (5)$$

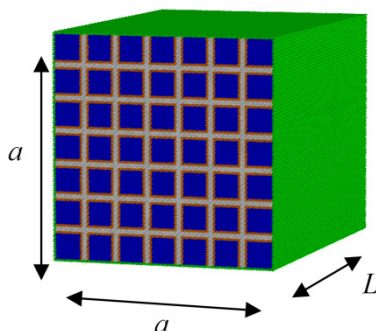


**Figure 10.** Schematic diagram of the fibril aggregate

Thus fibril aggregates with different lateral dimensions produce different specific surface areas. However this theory is limited since infinitely large objects yield specific surface areas too small to measure. Given that the hydroxyl groups on the fibril aggregate surface are the only functional groups initially available for further reaction, the question that arose from the above computation is whether the specific surface area measured using CP/MAS  $^{13}\text{C}$ -NMR could be related to a measure of chemical reactivity. To answer this, a series of reactivity studies were carried out on high purity pulp samples (i.e. 96% $\alpha$  dissolving pulp and cotton linters).

	LFD (nm)	LFAD (nm)	SSA ( $\text{m}^2/\text{g}$ )
<b>Cotton linters</b>	$7.1 \pm 0.1$	$47 \pm 2$	53
<b>Commercial 96%<math>\alpha</math></b>	$4.04 \pm 0.04$	$28 \pm 1$	89

**Table 3.** LFD (nm), LFAD (nm) and Specific Surface Area (SSA) in  $\text{m}^2/\text{g}$  for dissolving pulp samples

The LFD for the cotton linters cellulose is 7.1 nm. The native cellulose LFD is larger than the commercial produced dissolving pulp sample (average ca. 4 nm). The LFAD for the cotton linters cellulose was  $47 \pm 2$  nm compared to the commercial dissolving pulp sample i.e.  $28 \pm 1$  nm. For a larger LFAD, evident in Table 3, there is a smaller specific surface area. This implies that there is a smaller specific surface area available for chemical reaction.

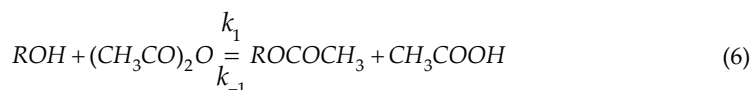
#### 1.2.6. The application of CP/MAS $^{13}\text{C}$ -NMR for determining initial reaction rates of dissolving pulp samples

The initial acetylation process depends on the accessibility of cellulose fibres and the susceptibility of individual cellulose I surfaces. Cellulose acetate is obtained from cellulose through the substitution of its cellulosic hydroxyl groups by acetyl groups. The properties of cellulose acetate depend on its degree of substitution, i.e. the average number of acetyl groups per anhydroglucose unit, and on the substituent distribution at three possible sites of anhydroglucose unit and along the length of cellulose chain [45]. The control of the acetylation time can be an important aspect to the variable degree of acetylation and the physical structure of cellulose acetate formed [46]. The fibrous conversion method also

provides partially acetylated cellulosic materials. Investigators prepared a paper with improved wet strength and dimensional stability from partially acetylated cellulose fibres [47]. Others studied the homogeneous acetylation process for Valonia and tunicate cellulose samples at the initial un-dissolved stage by CP/MAS <sup>13</sup>C-NMR, FT-IR and electron microscopy [48]. As a result, it was found that acetylation proceeds from the surface to the core of each microfibril and the I $\alpha$  crystals undergo acetylation more rapidly than the I $\beta$  crystals. Since the acetylated surface is expected to provide improved adhesion with hydrophobic matrices, use of partial acetylation of cellulosic fibres has been intensively studied as reinforcing elements for composite materials [49, 50].

To test the hypothesis that the specific surface area determined by the CP/MAS <sup>13</sup>C-NMR technique relates to chemical characteristic of the material, an attempt was made to correlate reaction rate ratios to ratios of specific surface areas determined by NMR. Acetylation experiments were performed with commercial 96% $\alpha$  Eucalyptus dissolving pulp and cotton linters. These samples are of high purity with respect to cellulose and differ significantly in their specific surface areas. Both samples were oven dried prior to acetylation. The hypothesis was based on the assumption that during the heterogeneous acetylation of cellulose, only hydroxyl groups situated at the surface of fibril aggregates are directly exposed to the surrounding liquid and hence, initially accessible to the reagent. Other hydroxyl groups reside either in the interior of fibrils or in the interior of fibril aggregates making them less accessible or inaccessible to the reagent.

The reaction scheme is illustrated below



*ROH* denotes the accessible hydroxyl groups on the cellulose,  $(CH_3CO)_2O$  denotes the acetic anhydride (*AA*), *ROCOCH<sub>3</sub>* denotes the formed cellulose acetate (*CA*) and *CH<sub>3</sub>COOH* denotes the formed acetic acid (*HAc*).  $k_1$  and  $k_{-1}$  denotes the forward and reverse reaction rates respectively. The general rate expression for the formation cellulose acetate can be given as (using abbreviations, brackets indicating concentrations)

$$\frac{d[CA]}{dt} = k_1[ROH]^a[AA]^b - k_{-1}[CA]^c[HAc]^d \quad (7)$$

Where  $[ROH]^a \propto SSA$

The experimental setup used a constant amount of cellulose for all reaction times, a large excess of acetic anhydride (*AA*) and acetic acid, and measured formed amounts of cellulose acetate (*CA*) only for short reaction times (initial reaction rates). The short reaction time effectively means that only a small fraction of all accessible hydroxyl groups were acetylated and that any reverse reaction rate can be neglected. The large excess of acetic anhydride used makes the concentration of acetic anhydride essentially constant throughout the course of the reaction. The large excess of acetic acid was necessary for two reasons. Firstly, it is

necessary for maintaining an approximately constant concentration of acetic acid throughout the reaction time (acetic acid is formed during the course of the reaction), and secondly acetic acid was needed due to its ability to swell cellulose. The swelling action of the acetic acid opens the pore system of the cellulose fibre wall making the specific surface area of the fibre wall cellulose accessible to the reagent acetic anhydride. This allows for the following approximations to be introduced.

$$\frac{d[ROH]}{dt} \approx 0 \quad (8)$$

$$\frac{d[AA]}{dt} \approx 0 \quad (9)$$

$$-k_{-1}[CA]^c[HAc]^d \approx 0 \quad (10)$$

Using these approximations pseudo-zero order reaction kinetics can be realized

$$\frac{d[CA]}{dt} = k_1[ROH]^a[AA]^b \approx k'[ROH]^a \approx k'' \quad (11)$$

The connection between the pseudo zero-order reaction rate ( $k''$ ) and the specific surface area, as determined from NMR LFAD measurements is given below, under the assumption that the exponent  $a$  in Equation (11) is equal to one.

$$k'[ROH] \approx k' \frac{\sigma MN}{V} = k'' \quad (12)$$

$[ROH]$  denotes the average volumetric concentration of accessible hydroxyl groups,  $\sigma$  denotes the specific surface area,  $M$  is the mass of the cellulose sample,  $N$  denotes the number of moles of hydroxyl groups per unit surface area and finally  $V$  denotes the sample volume. Keeping experimental conditions in agreement with the introduced approximations, keeping all parameters under experimental control equal only changing the cellulose substrate, a meaningful ratio of pseudo-zero order reaction rates can be formed. For substrates labelled A and B

$$\frac{k''_A}{k''_B} = \frac{k' \frac{\sigma_A MN}{V}}{k' \frac{\sigma_B MN}{V}} = \frac{\sigma_A}{\sigma_B} \quad (13)$$

Equation (13) relates the ratio of pseudo-zero order reaction rate determined from the kinetic experiments directly to the specific surface area determined from LFAD measurements. This means that it is possible to test if the LFAD value carries any information that is relevant to the chemical characteristics of the cellulose material, i.e. its behaviour during chemical modification. The system used for the acetylation was



formulated in agreement with the theoretical assumptions made to reach pseudo zero-order kinetics (Equations 6-13).

The specific surface area ratio, determined using CP/MAS <sup>13</sup>C-NMR, was compared to the pseudo zero order reaction rate ratio which was determined from the degree of acetylation. The question to be addressed was: does the supra-molecular structure of cellulose I, present in the 96% $\alpha$  grade dissolving pulp, influence the reactivity towards acetylation? This study used two pulp samples with different LFAD in the acetylation reaction i.e. 96% $\alpha$  commercial pulp and cotton linters cellulose. They were subject to acetylation at 40°C and 60°C. It was anticipated that the different pulp samples would have different specific surface areas and hence perform differently in the acetylation reactions. The aim of the experiment was to ascertain whether the ratio of specific surface areas for two 'different' pulp samples is similar to the ratio of the pseudo first order initial reaction rate constants. Table 1 presents the lateral fibril dimensions (LFD) and LFAD measurements, specific surface areas, pseudo first order initial reaction rate constant (k) at 40°C and 60°C for the cotton and commercial 96% $\alpha$  dissolving pulp samples. The graph of methyl intensity versus time reveals the pseudo first order initial reaction rate constant for each of the samples.

	SSA (m <sup>2</sup> /g)	k at 40°C	k at 60°C
<b>Cotton linters</b>	53	$1.4 \times 10^{-3} \pm 2 \times 10^{-4}$	$6 \times 10^{-3} \pm 6 \times 10^{-4}$
<b>Commercial 96%<math>\alpha</math></b>	89	$2.4 \times 10^{-3} \pm 3 \times 10^{-4}$	$11 \times 10^{-3} \pm 2 \times 10^{-3}$
<b>Cotton linters / Commercial 96%<math>\alpha</math> pulp (Ratio)</b>	$0.59 \pm 0.06$	$0.59 \pm 0.07$	$0.58 \pm 0.09$

**Table 4.** Summary of specific surface area ratio compared to initial reaction rate constant ratio computed from LFAD and density of cellulose

The pseudo zero order initial reaction rate constant ratio and specific surface area ratio for the commercial 96% $\alpha$  and cotton linters cellulose are presented in Table 4. The results show that the pseudo-zero order rate constant ratio is  $0.59 \pm 0.06$  with the ratio of specific surface area at 40°C being  $0.59 \pm 0.07$  and at 60°C being  $0.58 \pm 0.09$ . This shows that the ratio of initial reaction rate constants,  $k(\text{cotton linters})/k(\text{commercial } 96\%\alpha)$ , reproduce the ratio of specific surface area for both 40°C and 60°C reaction temperatures. This implies that:

1. Pseudo zero order initial reaction rate ratio is related to specific surface area ratio for two different substrates and
2. The pseudo zero order initial reaction rate constant ratio is independent of the temperature at which the acetylation reaction is performed.

A further comparison of acetylated sample analysis involved the use of <sup>1</sup>H-NMR. It was envisaged that it would provide a rapid result for the initial reaction rate constant compared to CP/MAS <sup>13</sup>C-NMR. The dried acetylated pulp samples were placed in deuterated chloroform. In theory, the acetylated surfaces should dissolve in deuterated chloroform with the solid or non-acetylated material filtered. The dissolved acetylated

pulp is then analysed by solution state NMR. The graph of acetyl intensity (cellulose triacetate) vs. time gives the initial reaction rate constant [51]. Table 5 shows a comparison of the different processes involved in the analysis of acetylated material by CP/MAS  $^{13}\text{C}$ -NMR and  $^1\text{H}$ -NMR.

CP/MAS $^{13}\text{C}$ -NMR	$^1\text{H}$ -NMR
1. Commercial 96% $\alpha$ pulp, Cotton linters	1. Laboratory 96% $\alpha$ pulp, Cotton linters
2. Acetylated at 40°C for 3, 6, 9 and 12 minutes.	2. Acetylated at 40°C for 10, 15, 20 and 25 minutes, dissolved in deuterated chloroform, undissolved material filtered off [50]
3. Packed in the rotor and run on the CP/MAS $^{13}\text{C}$ -NMR at ca. 6 hours a sample.	3. Run on the Proton NMR at ca. 2 minutes a sample.

**Table 5.** Comparison of sample preparation and analysis

The preliminary  $^1\text{H}$ -NMR reactivity study carried out on 96% $\alpha$  pulp samples and cotton linters showed that the short reaction times, 3; 6 and 9 minutes, did not provide any signal intensity. The experiment was thus performed at 10, 15, 20 and 25 minutes. Following first order reaction kinetics at short reaction times, the initial reaction rate constant was determined from a plot of cellulose triacetate signal intensity against time.

	Specific surface area ratio ( $\text{m}^2/\text{g}$ )	Initial reaction rate constant ratio determined by CP/MAS $^{13}\text{C}$ -NMR	Initial reaction rate constant ratio determined by $^1\text{H}$ -NMR
<b>Cotton linters / Commercial 96%<math>\alpha</math> pulp</b>	$0.59 \pm 0.06$	$0.55 \pm 0.12$	$0.60 \pm 0.05$

**Table 6.** Summary of results for specific surface area ratio vs. initial reaction rate constant ratio determined by CP/MAS  $^{13}\text{C}$ -NMR and  $^1\text{H}$ -NMR at 40°C

Table 6 highlights the results showing the comparison of the two techniques to determine initial reaction rate constant ratios. The specific surface area was determined from LFAD measurements using CP/MAS  $^{13}\text{C}$ -NMR. The pseudo initial rate constant ratio determined by CP/MAS  $^{13}\text{C}$ -NMR ( $0.55 \pm 0.12$ ) and first order reaction rate constant ratio determined by solution state  $^1\text{H}$ -NMR ( $0.60 \pm 0.05$ ) is related to the ratio of specific surface area ( $0.59 \pm 0.06$ ) of the acetylated materials. Results indicate that the initial reaction rate constant ratio is proportional to the specific surface area ratio for the cellulose pulp samples. This shows that specific surface area is related to initial reactivity to acetylation. It is thus possible to use solution state  $^1\text{H}$ -NMR to give an indication of initial reaction rate constants for acetylation.

## Author details

Viren Chunilall

*Council for Scientific and Industrial Research,  
Forestry and Forest Products (CSIR-FFP), Congella, Durban, South Africa*

Tamara Bush

*Department of Chemistry, University of KwaZulu-Natal, Durban, South Africa*

Per Tomas Larsson

*Innoventia AB, Stockholm, Sweden*

*Wallenberg Wood Science Centre, KTH Royal Institute of Technology, Stockholm, Sweden*

## Acknowledgement

The Council for Scientific and Research Council (CSIR) and Sappi Saiccor are acknowledged for financially supporting the project. P.T.L. acknowledges the Wallenberg Wood Science Centre in Sweden for financial support. The host company Innventia AB, Sweden, where the solid state NMR work was conducted is also acknowledged.

## 2. References

- [1] Sjöström E. Wood Chemistry – Fundamentals and Applications, 2nd ed. Academic Press; 1993
- [2] Gullichsen J. In: Gullichsen J. (ed) Papermaking Science and Technology, Chemical Pulping 6A. Fapet Oy: Jyväskylä; 2000.
- [3] Liitiä T. Application of modern NMR spectroscopic techniques to structural studies of wood and pulp components. PhD thesis. University of Helsinki; 2002.
- [4] Krässig HA. Cellulose - Structure, Accessibility and Reactivity. Polymer Monographs M. B. Huglin. Amsterdam, Gordon and Breach science publishers, Vol. 11; 1996.
- [5] Sarko A. Cellulose - How much do we know about its structure. In: Kennedy J F. (ed) Wood and Cellulose: Industrial utilization, biotechnology, structure and properties Chichester, UK: Ellis Horwood; 1987. p55-70.
- [6] Larsson PT, Hult E, Wickholm K, Pettersson E, Iversen T. CP/MAS  $^{13}\text{C}$  NMR spectroscopy applied to structure and interaction studies on cellulose I. Solid state NMR 1999; 15, 31-40.
- [7] Karlsson H. Fibre guide – Fibre analysis and process applications in the pulp and paper industry. AB Lorentzen & Wettre; 2006.
- [8] Gierer J. Chemistry of delignification Part 1: General concept and reactions during pulping, Wood Sci. Technol. 1985; 19, 289-312.
- [9] Funaoka M, Chang VL, Kolppo K, Stokke DD. Comparison of condensation reactions at  $\text{C}_\alpha$  positions in kraft and acid sulfite delignification of Western hemlock, Bull. Fac. Bioresources 1991; 5, 37-44.

- [10] Fengel D, Wegener G. Wood Chemistry, Ultrastructure, Reactions, Walter de Gruyter; 1984.
- [11] Uhlmann T. Ullmann's encyclopedia of industrial chemistry. Paper and Pulp. 1991; 18 (A).
- [12] Permanganate number of pulp, Tappi T214 wd-76 (UM-251), Tappi Press, Atlanta.
- [13] Acid insoluble lignin in wood and pulp, Tappi TM 222, Tappi Press, Atlanta.
- [14] Viscosity of pulp, Tappi T230 om-94, Tappi Press, Atlanta.
- [15] Röhring J, Potthast A, Rosenau T, Lange T, Ebner G, Sixta H, Kosma P. A Novel Method for the Determination of Carbonyl Groups in Cellulosics by Fluorescence Labeling. 1. Method Development, Biomacromolecules 2002; 3(5) 959-968.
- [16] Copper number of pulp, paper and paperboard, Tappi T430 OM 94, Tappi Press, Atlanta.
- [17] Alkali solubility of pulp, Tappi T235 OM- 60, Tappi Press, Atlanta.
- [18] Davis MW. A rapid modified method for compositional carbohydrate analysis of lignocellulosics by high pH anion exchange chromatography with pulsed amperometric detection (HPAEC/PAD). J. of Wood Chem. Technol. 1998; 18(2) 235-252.
- [19] Fischer K, Koch R, Fischer M, Schmidt I. Characterization of cellulose and cellulose derivatives by SEC. Das Papier 1999; 53 (12) 722-727.
- [20] Mehring M. Principles of high resolution NMR in Solids. Second revised and enlarged edition of NMR - Basic Principles and Progress, Vol 11. Springer-Verlag; 1983.
- [21] Verlhac C, Dedier J. Availability of surface hydroxyl groups in Valonia and Bacterial cellulose. Journal of Polymer Science: Part A 1990; 28 1171-1177.
- [22] Tsuboi M. Infrared spectrum and crystal structure of cellulose. Journal of Polymer Science 1957; 25 159-171.
- [23] Rowland SP, Howley PS. Microstructural order in the developing cotton fibre based on availabilities of hydroxyl groups. J. Polym. Sci. Polym. Chem. Ed. 1985; 23 183-192.
- [24] Horikawa Y, Sugiyama S. Accessibility and size of *Valonia* cellulose microfibril studied by combined deuteration/rehydrogenation and FTIR technique. Cellulose 2008; 15 419-424.
- [25] Larsson PT, Wickholm K, Iversen T. A CP/MAS  $^{13}\text{C}$ -NMR investigation of molecular ordering in celluloses. Carbohydr. Res. 1997; 302 19-25.
- [26] Wickholm K, Larsson PT, Iversen T. Assignment of non-crystalline forms in cellulose I by CP/MAS  $^{13}\text{C}$ -NMR spectroscopy. Carbohydr. Res. 1998; 312 123-129.
- [27] Sanders KM, Hunter BK. Modern NMR Spectroscopy, Oxford/New York/Toronto: Oxford University Press; 1987.
- [28] Schaefer J, Stejskal EO. Carbon-13 NMR of polymers spinning at the magic angle. J. Ant. Chem. Soc. 1976; 98 1031-1033.
- [29] Larsson PT, Westlund P-O. Line shapes in CP/MAS  $^{13}\text{C}$ -NMR spectra of cellulose I, Spectrochimica Acta, Part A 2005; 62 539-546.

- [30] Malm E, Bulone V, Wickholm K, Larsson PT, Iversen T. The surface structure of well-ordered native cellulose fibrils in contact with water. *Carbohydrate Research* 2010; 345 97-100.
- [31] Wickholm K. Structural Elements in Native Celluloses. PhD thesis. Royal Institute of Technology (KTH), Sweden; 2001.
- [32] Hult E-L, Larsson PT, Iversen T. Cellulose Fibril aggregation-An inherent property of kraft pulps. *Polymer* 2001; 42 3309-3314.
- [33] Larsson PT, Popescu CM, Vasile C. A comparative CP/MAS <sup>13</sup>C-NMR and XRD study of the cellulose supra-molecular structure in softwood kraft pulp fibres. *Papíripar* 2008; 52 235-237.
- [34] Atalla RH, VanderHart DL. The role of solid state <sup>13</sup>C-NMR spectroscopy in studies of the nature of native celluloses. *Solid State Nuclear Magnetic Resonance* 1999; 15 1-19.
- [35] Sugiyama J, Vuong R, Chanzy H. Electron diffraction studies on two crystalline phases occurring in native cellulose from an algal cell wall. *Macromolecules* 1991; 24 4168-4175.
- [36] Heiner AP, Kuutti L, Teleman O. Comparison of the interface between water and four surfaces of native crystalline cellulose by molecular dynamics simulations. *Carbohydrate Research* 1998; 306 205-220.
- [37] Newman RH. Estimation of the lateral dimensions of cellulose crystallites using <sup>13</sup>C-NMR signal strengths. *Solid state Nucl. Magn. Res.* 1999; 15 21-29.
- [38] Jayme G. Mikro-Quellungsmessungen an Zellstoffen. *Wochenbl Papierfabr* 1944; 6 187-194.
- [39] Diniz Fernandes JMB, Gil MH, Castro JAMM. Hornification-its origin and interpretation in wood pulp samples. *Wood Sci. Technology* 2004; 37 489-494.
- [40] Nocanda X, Larsson PT, Spark A, Bush T, Olsson A, Madikane M, Bissessur A, Iversen T. Cross polarisation/ magic angle spinning <sup>13</sup>C-NMR spectroscopic studies of cellulose structural changes in hardwood dissolving pulp process. *Holzforschung* 2007; 61 (6) 675-679.
- [41] Oksanen T, Buchert J, Viikari L. The role of hemicelluloses in the hornification of bleached kraft pulps. *Holzforschung* 1997; 51 (4) 355-360.
- [42] Newman RH. Carbon 13 NMR evidence for the co-crystallization of cellulose as a mechanism for hornification of bleached kraft pulp. *Cellulose* 2004; 11 45-52.
- [43] Rebuzzi F, Evtuguin DV. Effect of Glucuronoxylan on the hornification of *Eucalyptus globulus* bleached pulps. *Macromol. Symp.* 2006; 232 121-128.
- [44] Kontturi E, Vuorinen T. Indirect evidence of supramolecular changes within cellulose microfibrils of chemical pulp fibres upon drying. *Cellulose* 2009; 16 (1) 65-74.
- [45] He J, Tang Y, Wang S-Y. Alkaline treatment of diacetate fibers and subsequent cellulase degradation. *Journal of Applied Polymer Science* 2008; 107, 2466-2474.

- [46] Barud HS, de Araujo Junior AM, Santos DB, de Assuncao RMN, Meireles CS, Cerqueira D A. Thermal behavior of cellulose acetate produced from homogeneous acetylation of bacterial cellulose. *Thermochimica Acta* 2008; 471 61–69.
- [47] Herdle LE, Griggs WH. Partially acetylated cellulose-its properties and potential applications. *Tappi* 1965; 48 103–107.
- [48] Sassi J-F, Tekely P, Chanzy H. Relative susceptibility of the I $\alpha$  and I $\beta$  phase of cellulose towards acetylation. *Cellulose* 2000; 7 119-132.
- [49] Kim D-Y, Nishiyama Y, Kuga S. Surface acetylation of bacterial cellulose. *Cellulose* 2002; 9 361-367.
- [50] Matsumura H, Glasser WG. Cellulosic nanocomposites. II. Studies by Atomic force microscopy. *Journal of Applied Polymer Science* 2000; 78 2254-2261.
- [51] Goodlett VW, Dougherty JT, Patton HW. Characterisation of cellulose acetates by nuclear magnetic resonance. *Journal of Polymer science Part A-1*. 1971; 9, 155-161.